Cu nanoparticles embedded on reticular chitosan-derived N-doped carbon: Application to the catalytic hydrogenation of alkenes, alkynes and N-heteroarenes

Nisrine Hammi, Shuo Chen, Christophe Michon, Sebastien Royer, Abdelkrim El Kadib

Cu nanoparticles embedded on reticular chitosan-derived N-doped carbon: application to the catalytic hydrogenation of alkenes, alkynes and N-heteroarenes

Nisrine Hammi,[a,b] Shuo Chen,[a] Christophe Michon,[a,c] Sebastien Royer,[a,*] and Abdelkrim El Kadib[b,*]

[a] Univ. Lille, CNRS, Centrale Lille, Univ. Artois, UMR 8181 – UCCS – Unité de Catalyse et Chimie du Solide, F-59000 Lille, France

[b] Euromed Research Center, Engineering Division, Euro-Med University of Fes (UEMF), Route de Meknes, Rond-point de Bensouda, 30070, Fès, Morocco.

[c] Université de Strasbourg, Université de Haute-Alsace, ECPM, CNRS, LIMA UMR 7042 25 Rue Becquerel, FR-67087 Strasbourg, France

* Corresponding authors: email address: A. El Kadib (a.elkadib@ueuromed.org); S. Royer (sebastien.royer@univ-lille.fr)

ABSTRACT

Applying biomass-waste as catalysts and catalytic supports is gaining a tremendous interest owing to its expected outcomes in terms of cost effectiveness and sustainability. In this context, we herein disclose a straightforward encapsulation of nanosized copper on hierarchically porous, biomass-derived nitrogen-containing carbon framework. Our approach uses chitosan - derived from the marine shell-fish wastes - as a cheap, sustainable carbon and nitrogen source, melamine as nitrogen provider and ethylenediaminetetraacetic acid as a cross-linker to induce the reticular network, much suitable for restricting the growth of the metal seeds. The resulting copper grown on nitrogen-doped carbon, bearing relatively large surface area (106 $m^2 \cdot g^{-1}$) and a large group of well-dispersed Cu nanoparticles (average of 2 nm) even with high Cu loading (41 wt%), exhibits catalytic activity for the hydrogenation of unsaturated double and triple carbon-carbon bonds and heteroaryles. This sustainable design of catalyst, using affordable copper and cheap biowaste, could discard palladium and other expensive elements loaded on tedious synthetic supports from the library of heterogeneous solids intended for fine chemical synthesis.

KEYWORDS

Copper nanoparticles; N-doped carbon; Chitosan; Hydrogenation catalysis.

1. INTRODUCTION

Catalytic hydrogenation is one of the most useful and widely applicable methodologies for the synthesis and manufacturing of industrial and fine chemicals, including materials and active pharmaceutical drugs. Typical examples are reductive transformation of unsaturated C=C double and C≡C triple bonds containing-molecules [1-4]. N-heterocycles [5], nitrocyclohexane [6], and the hydrogenation/hydrogenolysis of biomass-derived platform

molecules (e.g., fatty acids and triglycerides, furfural, 5-hydroxymethylfurfural, glycerol, etc.) [7]. Owing to their high capability for hydrogen activation, noble metal supported catalysts (e.g. platinum, palladium, rhodium, and ruthenium) display excellent activity and selectivity for a broad substrate scope [8]. Unfortunately, noble metal based catalysts suffer from scarcity and high cost. Alternative solutions to catalyze hydrogenation reactions rely on the use of non-noble transition metals (e.g. Cu, Co, Ni, Fe or Mn), which are more abundant and therefore of lower costs [9-13]. Interestingly, in some cases, these affordable metals encapsulated in microporous or mesoporous materials (zeolites, MOFs, carbon, etc.) exhibit good activity and stability during reduction transformation under mild conditions, sometimes even superior to noble-metal based catalysts [14,15]. This activity enhancement is often rationalized by the confinement effect and the suppression of the metal propensity for clustering and leaching that are the main reasons for catalyst deactivation.

Among those of interests, Cu-based catalysts have attracted considerable attention, the reduced cost being the driving force for their applications in a variety of organic transformations [16,17,18,19]. However, the thermal instability of Cu constitutes a serious impediment as the high surface energy of nanosized copper results in their aggregation and coarsening into large crystals during the thermal steps necessary for solid preparation, conditioning, and even during catalysis [20]. Copper tethered on silica, zeolite and alumina have been applied in different catalytic reactions, including the hydrogenation of double and triple carbon-carbon bonds as well as nitrogen-containing heterocycles [21,22,23]. Recent trends have revealed that embedding copper nanoparticles in a cleverly-designed supports [24], such as texturally-engineered nitrogen-doped carbon framework imparts the solid material with improved catalytic activity and stability [25]. Notably, incorporation of

nitrogen in carbon nanostructures provides strong coordinating sites for metal deposition, prevents coarsening into large crystals and reduces severe leaching that may occur during catalysis [26,27]. Additional advantages could be associated to the alteration of the electronic properties of the carbon supports that could be required for electrocatalysis [28]. However, to the best of our knowledge, copper grown on nitrogen-doped carbon has not been evaluated for hydrogenation so far [29], while catalytic hydrogenation using cobalt supported on carbonized chitosan was already proposed [30-33].

Among the well-established carbon precursors, biomass possesses hierarchical structures and periodic patterns that replicate in the resulting carbon materials at different scales, including the macro-, micro- and nano-sized dimensions. Distinctively, chitosan is a cheap, abundant, and renewable polysaccharide that hold in its structure nearly 7 wt% of nitrogen. This makes chitosan one of the most interesting bio-waste that can be used for the preparation of N-doped carbon materials without additional post-synthetic steps necessary for nitrogen fixation [34]. The properties of chitosan relate to its multiple functional groups, including hydroxyl, amino, and acetamido groups and to its poly-electrolytic and sugar-based polymeric properties. Several synthetic procedures, alone or in combination, have been used for the transformation of chitosan into different carbon materials. Among them, hydrothermal or solvothermal approaches followed by pyrolysis under inert atmospheres are the mostly used [35]. Given the thermally induced evolution of chitosan skeleton during the carbonization process, the precise control of the experimental parameters is a crucial matter. In most cases, inert gas atmosphere is required, and the choice of the temperature range and its variation is also pivotal depending on the nature of the target carbon materials. Herein, we report the rational design of a Cu supported on nitrogen doped carbon (Cu-NC)

catalyst using bio-waste derived chitosan as a sustainable and cost-effective carbon and nitrogen source.

As schematized in Scheme 1, the CuNC catalysts were prepared through sequestration of copper element in a colloidal solution of cross-linked chitosan. Melamine was also introduced to further enrich nitrogen content in the material framework and the mixture was cross-linked, hydrothermally treated and then thermally-annealed under nitrogen atmosphere at 700 °C to simultaneously convert the polysaccharide skeletal into nitrogen-containing carbon framework and to reduce the entrapped copper ions into small-sized metallic particles. With materials displaying copper loading up to 41 wt%, we next investigated the hydrogenation activity of the resulting solids for alkenes, alkynes as well as N-heterocycles under batch reaction conditions. Our results demonstrate that even at high copper loading, the growth and dispersion of copper nanoparticles remain controlled within N-doped carbon support. The following approach enabled access to sustainable, cost-effective, and active catalytic systems for the hydrogenation of unsaturated organic compounds.

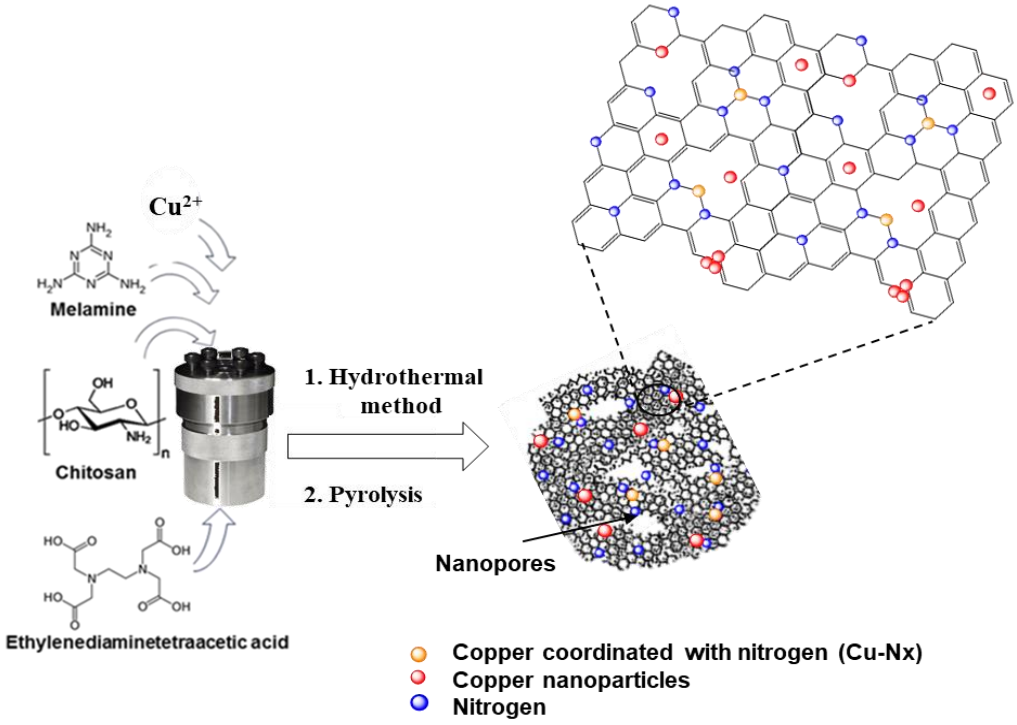

Scheme 1. Multistep preparation procedure using the three precursors (chitosan, melamine and ethylenediaminetetraacetic acid) for the synthesis of copper nanoparticles supported on N-doped carbon material.

2. EXPERIMENTAL SECTION

General procedure for CuNC catalysts synthesis

N-doped copper-carbon composites were prepared by the following procedure: chitosan (0.400 g) and ethylenediaminetetraacetic acid (0.080 g) were mixed in 64 mL of aqueous acetic acid (1 % v/v). Then, melamine (0.060 g) was added and the mixture was stirred for additional 3 h. An alcoholic solution of $Cu(NO_3)_2.3H_2O$ was next added according to the different molar ratio of NH_2:Cu (1:1, 1:2, 2:1) and the mixture was stirred for 24 h. The resulting solution was poured into a Teflon-lined autoclave, sealed and heated at 180 °C for 24 h. The powder was collected by centrifugation and washed three times with distilled water (3 × 20 mL). Finally, the obtained black solid was dried overnight at 80 °C. The dry solid was pyrolyzed at 700 °C under N_2 flow for 2 h

(with a ramp of 2 °C·min^{-1}). Samples were denoted as CuNC-x-700, where x represents NH_2:Cu ratio (x = 0.5, 1, 2). A non-cross-linked material was prepared by following the previous procedure, denoted as CuCS-700. Nitrogen doped carbon without Cu was prepared as a reference catalyst and denoted NC-700. Besides, in order to study the role of the nitrogen, one less nitrogen content carbon material was prepared by following the previous procedure except that melamine was not added. Moreover, a nitrogen-free carbon material was prepared by following the previous procedure but using rather polymeric alginate as source of carbon. The obtained materials were denoted CuNC-700 and CuC-1-700, respectively.

General procedure for CuNC catalyzed hydrogenation

Heterocycle, alkene or alkyne substrate (0.7 mmol, 1 eq.) and selected reduced catalyst (0.005 g for alkenes and alkynes, 0.010 g for heterocycles) were introduced in an autoclave of 100 mL, and isopropanol solvent (4 mL) was added. The autoclave was then filled with hydrogen at a pressure of 50 bar for heterocycles or 10 bar for alkenes and alkynes after 3 purges. The reaction mixture was then heated at 80 °C under stirring during the selected time. At the end of the reaction, autoclave was cooled then degassed. The crude reaction product was recovered after filtration over Celite and solvent evaporation under vacuum. After GC and GC-MS analyses, it was then purified by flash chromatography using petroleum ether and ethylacetate. Each reaction product was characterized by ^{1}H and ^{13}C NMR analyses.

Materials characterization

N_2 physisorption isotherms were recorded at -196 °C on a Micromeritics Tristar II automated gas sorption system. Before analysis, the samples were outgassed under dynamic vacuum at 300 °C for 8 h. Specific surface area was determined using the multipoint B.E.T. algorithm in the P/P_0 range from 0.25 to 0.4. The mesopore size distribution was determined by B.J.H. equation applied

to the desorption branch. Pore volume is determined on the adsorption branch at $P/P_0 = 0.98$. X-ray diffraction (XRD) was performed using a Bruker X-ray AXS D8 Advance diffractometer in Bragg-Brentano configuration and equipped with a LynxEye Super Speed detector. XRD patterns were recorded with Cu Kα radiation (λ = 0.154 nm, 40 kV, 30 mA) in the 10–80° 2θ range with a 0.02° of 2θ step. Phase identification was made by comparison with the ICDD database. Micrographs from Transmission Electron Microscopy (TEM) were conducted on a JEOL 2100 UHR, operated at 200 kV with a LaB6 source and equipped with a Gatan 832 CCD camera. Scanning electronic microscopy (SEM) images were obtained using a JEOL JSM-7800F LV. A KRATOS Axis Ultra spectrometer operated under ultrahigh vacuum condition, using a twin Al X-ray source (1486.6 eV) at a pass energy of 40 eV, was used for the X-ray photoelectron spectroscopy (XPS) analyses. The solid, in the form of pellet, was fixed on a copper holder with copper tape. The binding energy values were estimated, positioning the C 1s peak of contaminant carbon at a B.E. of 285.0 eV. The Casa XPS software package was used for data analysis. H_2-TPR was conducted on a Micromeritics AutoChem II 2920 chemisorption analyser, equipped with a TCD. Before H_2-TPR run, a catalyst mass fixed to ~60 mg, was inserted in a quartz reactor and degassed under inert gas. A flow of 5 vol.% H_2/Ar was stabilized at a total flow rate of 50 mL/min, and the catalyst was heated from 50 °C to 700 °C with rampe of 10 °C/min. CO_2-Temperature Programmed Desorption (CO_2-TPD) experiments were carried out with the same instrument. A sample mass of ~100 mg was degased under inert gas flow (He, 30 mL/min) for 30 min at 300 °C before being cooled to 50 °C. Then 5% CO_2 (30 mL/min) was fed to the catalyst for 30 min at 50 °C, the oven temperature was increased to 700°C with heating rate of 10 °C/min. The gas flow at the reactor outlet is analyzed using a TCD detector and a mass spectrometer (m/z= 32, O_2; m/z=18, H_2O; m/z=28, N_2; m/z = 44, CO_2). X-band EPR spectra were recorded at room temperature using

a Brüker ELEXSYS E500 spectrometer. EPR settings were respectively 5 mW for microwave power and 2 G for amplitude modulation.

RESULTS AND DISCUSSION

As depicted in Scheme 1, the carbon framework was constructed using three components: chitosan derived marine biopolymer (extracted from the exoskeleton of crustaceans' shell waste) as the main carbonaceous precursor, melamine (MA) as nitrogen provider and ethylenediaminetetraacetic acid (EDTA) as an appropriate cross-linker to bridge the two precursors in the same network through amide bonding while sequestrating at the same time the copper precursor ($Cu(NO_3)_2.3H_2O$). The incorporation of Cu(II) species was achieved by adding different amounts of $Cu(NO_3)_2.3H_2O$ in order to vary the final content of the metal with respect to the carbon support. The resulting solution was subjected to hydrothermal treatment for further condensation and densification. The harvested carbonaceous gel was annealed at 700 °C, which is commonly used for such carbonization purpose and which is far above the main decomposition steps of the organic matter encountered below 400 °C (Fig. S1) [35]. ICP analysis reveals a copper weight content of 19 wt% for **CuNC-0.5-700**, 41 wt% for **CuNC-1-700** and 59 wt% for **CuNC-2-700**, following the increase of the metal loading in the starting solutions. Surface functionalities of the resulting materials were studied using FTIR spectroscopy among other techniques (Fig. S2). Absorption bands at 3694-3537 cm^{-1} ascribed to the asymmetric and symmetric stretching vibrations of NH groups and OH groups are observed for copper-free NC-700 material [36]. Comparatively, less resolved signals are observed in the samples containing copper, suggesting the involvement of the latter in the carbonaceous decomposition through C-C cleavage. The absence of characteristic bands of native chitosan films (1548 cm^{-1} and

1634 cm^{-1} for the glucosamine and N-acetylglucosamine units, respectively) in **CuNC-1-700**, confirms their consumption during pyrolysis. Besides, the presence of nitrogen in **CuNC-1-700** was preliminary evidenced by the appearance of a broad vibrational mode at 2024 cm^{-1}, typical of C≡N bond [37]. Furthermore, **CuNC-1-700** showed broad vibrational modes at 1488 cm^{-1} and 734 cm^{-1} attributed to the benzylic ring mode and C=O bond, respectively. Elemental analyses confirm the persistence of nitrogen after thermal annealing treatment, reaching a value of 5.65 wt% for **NC-700**, 7.67 wt% for **CuNC-1-700** and 7.82 wt% **CuNC-2-700**. This endogenous nitrogen enrichment, supplied mainly by the use of chitosan as a bio-based carbohydrate shellfish waste, is one of the most important features for this strategy, as nitrogen doping often necessitates the use of ammonia or other corrosive substrates that could reduce the sustainability of the process [27].

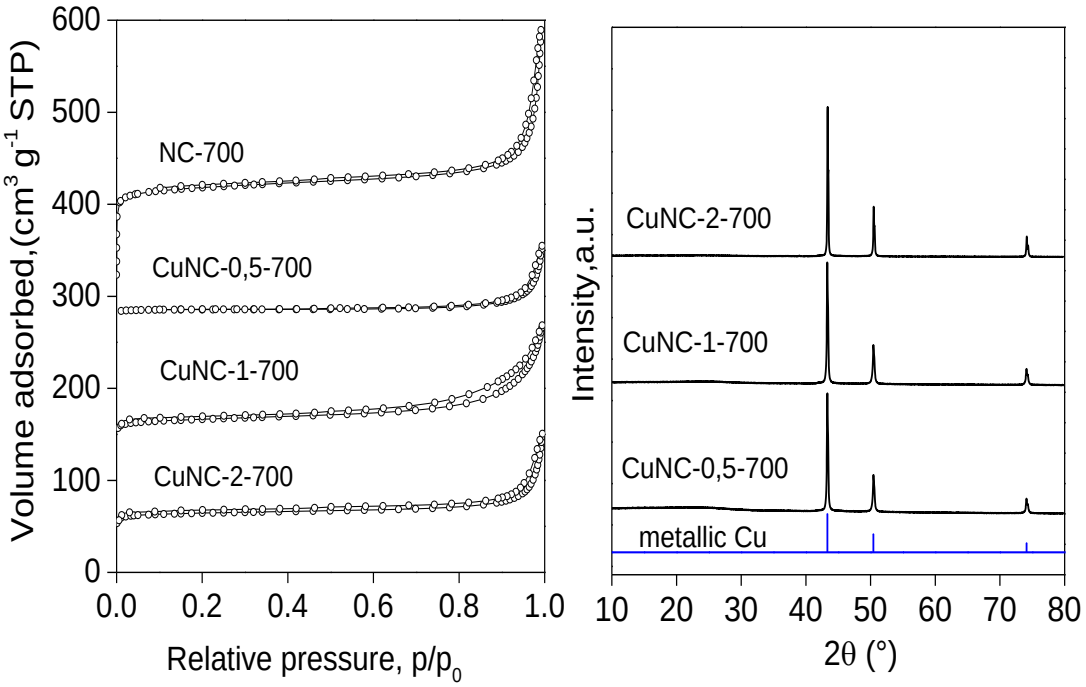

Fig. 1. N_2 adsorption-desorption isotherm (a) and X-ray diffraction patterns (b) obtained for the **NC-700** and **CuNC-x-700** materials.

N_2 adsorption-desorption isotherms obtained for **NC-700** and **CuNC-x-700** are presented in Fig. 1a and the textural parameters are listed in Table S1. **NC-700** shows a surface area of 447 $m^2.g^{-1}$ while a significant decrease was observed after metal incorporation (19 wt% of Cu) reaching 203 $m^2.g^{-1}$ for **CuNC-0.5-700** (Table S1). When Cu loading increases up to 41 wt% for **CuNC-1-700** and 59 wt% for **CuNC-2-700**, the decrease of the specific surface area become more significant, giving 106 $m^2 \cdot g^{-1}$ and 97 $m^2 \cdot g^{-1}$ respectively. This decrease is clearly related to the introduction of the metal into the carbon framework. Indeed, carbonization of the metal-free mixture provides large mesopores which extend to the macroporous domain while the presence of the metal triggers the formation of mesopores in addition to residual macropores, as reflected by the isotherm shape, remaining of type II with H3 type hysteresis (Fig. 1a). The presence of hierarchical porosity is of tremendous interest in catalysis considering the mass transfer and adsorption of the reactants (and products) to (and from) active sites as well as the long-term stability of metal nanoparticles [38]. Cross-linking of the framework seems to be beneficial for sustaining the porous network during carbonisation, thereby providing nearly 106 $m^2 \cdot g^{-1}$ as accessible surface area while only half of this value (54 $m^2.g^{-1}$) was recorded during carbonisation of the non-cross-linked material, denoted as **CuCS-700**. Additionally, an increase in micropore surface is observed with the metal loading (Table S1), the microporous surface representing 43% of the total surface for **CuNC-2-700**.

In XRD, typical diffraction patterns of metallic copper were observed at 43.3°, 50.4°, and 74.1° (ICDD file n°04-0836) for the three samples after pyrolysis step at 700 °C (Fig. 1b). The average size of the crystalline copper, estimated by Scherrer equation, increases with the metal loading, from 20 nm for **CuNC-0.5-700** to 29 nm for **CuNC-1-700**, and to 35 nm

for **CuNC-2-700**. Crystalline copper nanoparticles grown on carbonized chitosan without cross-linking (EDTA) in **CuCS-700** or without using melamine in **CuNC-700**, display similar diffraction patterns, but giving a large crystal size of 48 nm and 37 nm, respectively. This confirms the proposed role of EDTA as a cross-linker to sequestrate the growing metal leading to high particles dispersion [39], and the use of the nitrogen for stabilizing small-sized metal species in the materials [40]. No copper oxides or other crystalline phase were observed, indicating selective formation of crystalline copper nanoparticles. For a further evidence of the role of nitrogen belonging to chitosan in this catalyst design, we also explored the synthesis of copper loaded alginate as a nitrogen-free polysaccharide analogue. XRD of the resulting **CuC-1-700** displays other crystalline phases (assigned to CuO and Cu_2O) with the average size of the crystals being calculated to 66 nm. This definitely indicates the pivotal role of chitosan as macro-chelating ligand to stabilize molecular copper and to restrict later the growth of copper nanoparticles. The highest affinity of nitrogen to copper is well documented [15, 41, 42] and is for instance at the basis of the use of chitosan as sorbent for copper removal from contaminated water medium.

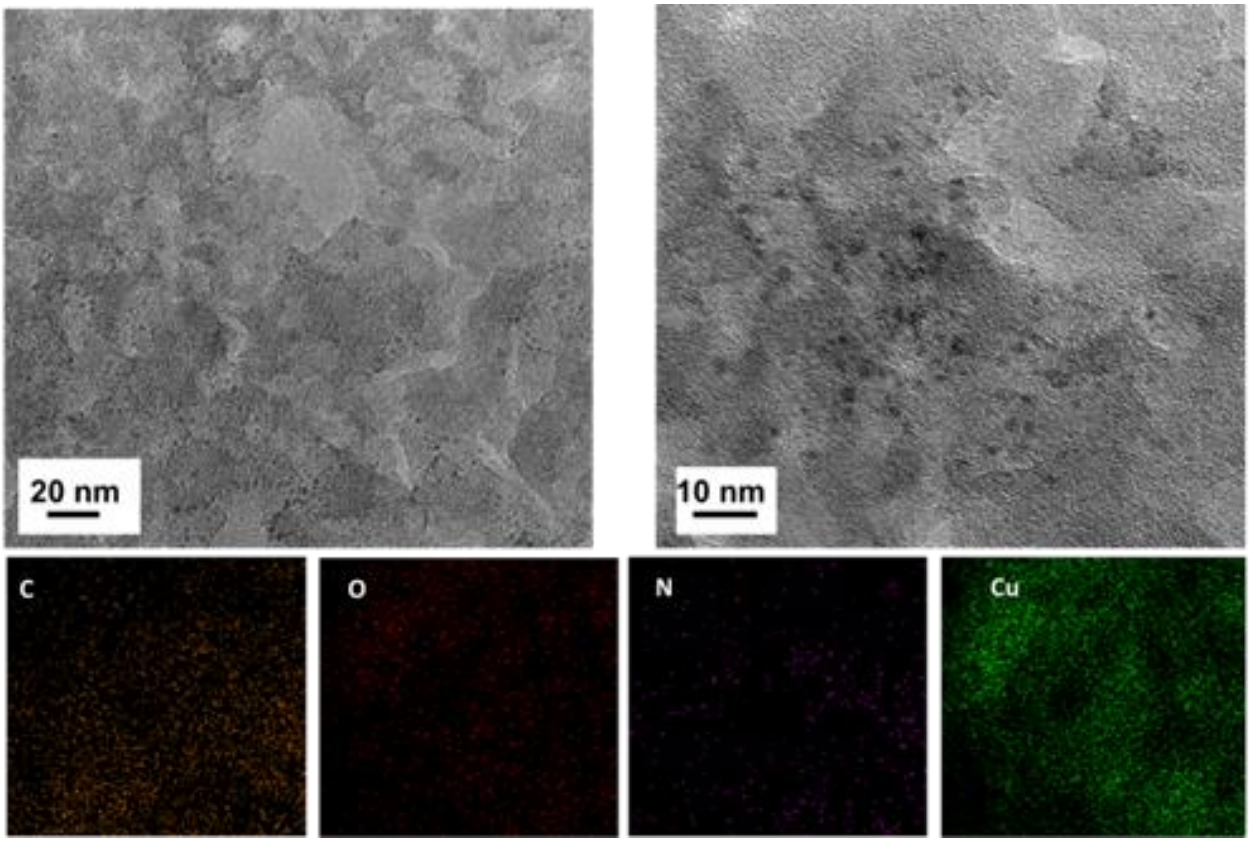

Fig. 2. HRTEM images and elemental mapping of C, Cu, O and N obtained for **CuNC-1-700**.

Scanning electronic microscopy analyses evidenced the formation of dispersed copper nanoparticles within the carbonized chitosan framework (Fig. S3). The size of the copper nanoparticles was found to be enhanced while increasing the metal loading, and therefore providing an excess of copper as respect to the available nitrogen coordinating sites. Indeed, the average size increases from 25 nm for **CuNC-0.5-700** to 66 nm for **CuNC-1-700** and to 120 nm for **CuNC-2-700** (Fig. S4). Transmission electronic microscopy analysis under higher magnification shows the presence of small nanoparticles with an average size of 2 nm (Fig. 2 and Fig. S5), while the scanning electronic microscopy allows to evidence the formation of larger size – external – copper particles (Fig. S4a). The presence of both small particles and external clustered particles could be associated to their growth in different environments: e.g., in micropores-mesopores versus macropores, and/or inside versus

outside the porous framework or near to the pore entrances. Herein, the observed clustering is quite expected considering the high metal loading that was embedded inside, reaching 52 wt% in the case of **CuCN-2-700** (Fig. S4c). The element mapping results however confirmed the homogeneous elemental dispersion for nitrogen, carbon, oxygen together with copper without phase separation or bulk segregation at nanoscale level (Fig. 2).

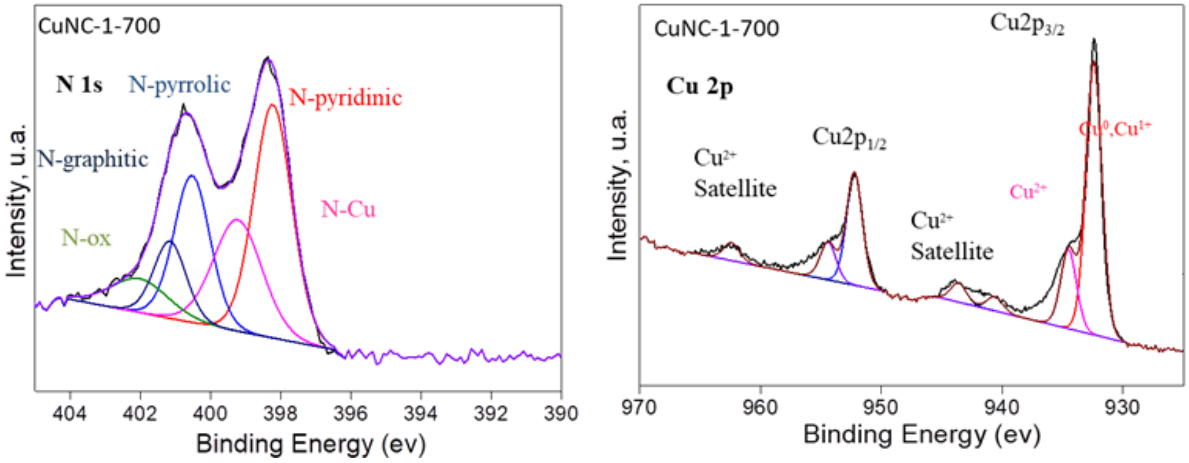

Fig. 3. XPS results of **CuNC-1-700**

XPS measurements were further performed to identify the electronic environment of nitrogen and copper species in the **CuNC-x-700** samples as well as the oxidation state of the metal. XPS patterns of **CuNC-0.5-700**, **CuNC-1-700** and **CuNC-2-700** exhibit four typical core levels signals for C 1s, N 1s, O 1s and Cu 2p (Fig.S6 and Fig. 3, Table S2). Decomposed N 1s spectrum features an extra signal (399.2 eV) for graphitic N species, attributed to the interaction of Cu species with pyridinic N, which could be explained by the formation of a Cu complex with involvement of pyrrolic nitrogen causing a shift of the pyrrolic line toward the position of the graphitic line [40]. Graphitic N was reported to play a crucial role as active species in oxygen reduction [41]. Besides, pyridinic N and pyrrolic N serve as metal coordination sites due to their lone-pair electrons [42-46]. Decomposition of Cu 2p XPS spectrum reveals major peaks of Cu 2p3/2 at 932.4 eV and Cu 2p1/2 at 952.2

eV indicating the presence of metallic copper [47], as a result of the successful carbo-reduction of Cu^{2+} during the pyrolysis process. Meanwhile, the peaks at 934.5 eV and at 954.4 eV in combination with the satellite peaks at 940.6 eV and 943.6 eV are typical characteristics of CuO [48], which is probably formed upon exposure to air after carbo-reduction step.

Fig. S7 presents the CO_2-TPD profile of **CuNC-1-700**. The peak at 100-200 °C originates from a weekly basic site whereas that at 300-700 °C corresponds to a strong basic site [49]. The basic sites are associated with the N-H species in N-doped carbon, which would serve as anchoring sites to interact with copper species as indicated by the XPS and FT-IR results [50]. The reducibility of **CuNC-1-700** and **CuC-1-700** was characterized by H_2-TPR. As presented in Fig. S8, the reduction peaks in the low temperature range of 150-350 °C can be linked to the reduction of Cu^{2+} to Cu^0 NPs [51]. The reduction temperature of CuO NPs strongly depends on the support-metal interaction and the metal dispersion. The lower reduction temperature exhibited by **CuNC-1-700** at 171 °C than that of **CuC-1-700** at 225-335 °C could be assigned to stronger support-metal interaction and higher copper dispersion [52].

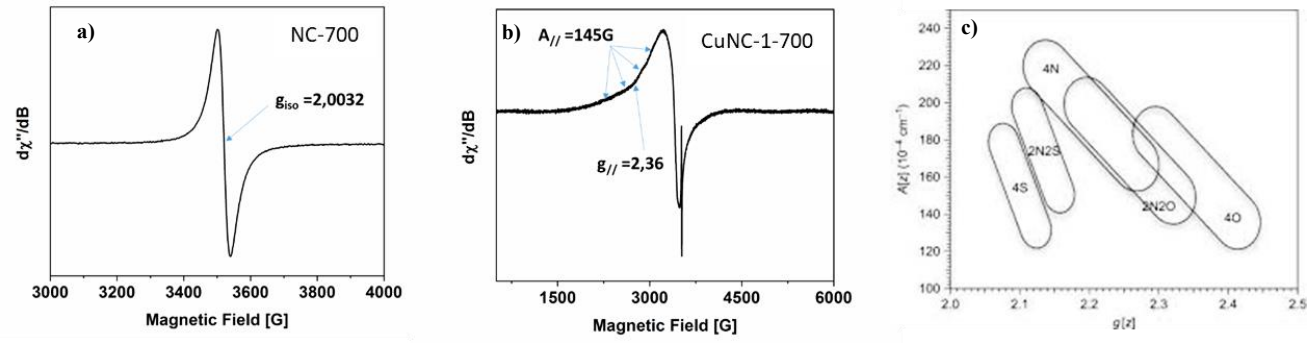

Fig. 4. EPR spectra of NC-700 and CuNC-1-700 (a,b); Peisach-Blumberg analysis of CuN-1-700 EPR spectra (c).

In order to have better insight about insertion in the carbon structure, CW EPR experiments have been performed at room temperature. Fig.4 presents the EPR spectra and Peisach-Blumberg analysis of NC-700 and CuNC-1-700. The pristine sample exhibits an isotropic signal centred at g=2.0032 indicating the presence of carbon centred paramagnetic species [53]. After copper insertion we can observe the presence of copper species which displays an axial symmetry, and in the parallel region the hyperfine coupling between the electron spin of Cu^{2+} (S=1/2) and its nuclear spin (I=3/2). The hyperfine coupling was measured with a value A//=145G and the corresponding g value is 2.36. Such a value compared to the diagram of Peisach-Blumberg indicates at least that one or two nitrogens can participate to the copper coordination sphere complexes [54].

All of the resulting materials were tested in the hydrogenation of quinoline (molecule 1a, Table 1) at a relatively mild temperature (80 °C) under 50 bar hydrogen in isopropanol (iPrOH) (Table 1). No catalytic activity was observed for the metal-free **NC-700**, discarding any contribution through metal-free hydrogenation from the support and confirming the necessary presence of the metal as active site (Table 1, entry 1). Furthermore, no conversion was observed without the use of a hydrogen pressure excluding a possible transfer hydrogenation using iPrOH as hydrogen donor and the quinoline substrate **1a** as a base (Table 1, entry 2). The highest conversion was obtained with the **CuNC-1-700** sample compared to **CuNC-0.5-700** and **CuNC-2-700** (Table 1, entries 3-5). Though featuring the highest metal content, the latter suffered from severe aggregation of the clusters to 120 nm (Figure S4a) which resulted in poor catalytic activity. Nitrogen-free **CuC-1-700**, obtained through alginate route, exhibited poor catalytic activity because of its failure to selectively provide copper nanoparticles (Table 1, entry 6). **CuCS-1-700** obtained by carbonization route, without cross-linking displayed also moderate catalytic

activity (26%) probably due to its marginal surface area that hamper the diffusion of the reactants and products during catalysis (Table 1, entry 7). **CuNC-1-700a**, obtained by air oxidation of **CuNC-1-700** at 200 °C and exhibiting only CuO phase as indicated by the high angle XRD result (Fig. S9), afforded only a low conversion of 12% (Table 1, entry 8). This further confirmed that Cu^0, instead of Cu^{2+}, served as the main active source. The high catalytic performance of **CuNC-1-700** could thus be assigned to the presence of highly dispersed Cu^0 particles which expose a broad active surface to the substrate. Besides, the nitrogen species complexed with the surface metallic sites may act as the hydrogenation activity promoter owing to the electron transfer between the N species and the metallic centres, which subsequently benefited the high catalytic activity.

Table 1. Catalytic results obtained in the hydrogenation of quinoline **1a** using different catalysts.

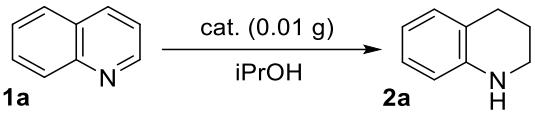

Entry[a]	Catalyst	H_2 (bar)	T (°C)	t (h)	Conversion (%)[a,b]
1	NC-700	50	80	61	0
2	CuNC-0.5-700	0	80	61	0
3	CuNC-0.5-700	50	80	61	74
4	CuNC-1-700	50	80	61	82
5	CuNC-2-700	50	80	61	13
6	CuC-1-700	50	80	61	11
7	CuCS-1-700	50	80	61	26
8	CuNC-1-700a	50	80	61	12

[a] Reaction conditions: quinoline (0.7 mmol), catalyst (0.010 g), iPrOH (4.0 mL), H_2 (50 bar), T (80 °C), t (61 h).
[b] Determined by GC and GC-MS.

It could be noted that a catalyst with a low loading of copper metal contained small metal particles, and quinoline hydrogenation over CuNC clearly showed a size-dependent

catalytic activity. Indeed, CuNC with small metal nanoparticles showed much higher activity than the one with larger nanoparticles (Table S3).

Following this catalyst screening test, **CuNC-1-700** was selected for the catalytic hydrogenation of other N-heterocycles and carbon-carbon double and triple bonds (Table 2, 3 and 4). First, the catalyst was assessed for the hydrogenation of challenging N-heterocycles (Table 2) which are important structural motifs found frequently in pharmaceuticals and agrochemicals [55]. The performed hydrogenation reactions were completely selective without any semihydrogenation or condensation by-products.

Interestingly, hydrogenation of quinoline **1a**, 2-methyl-quinoline **1b** and phenanthridine **1c** afforded the corresponding reduced products respectively in 82, 77 and 75% yield within 61 h (Table 2, entries 1-3). Nearby quantitative yields were obtained for the hydrogenation of acridine **1d** and pyrazine **1e** over **CuNC-1-700** within 13 h (Table 2, entries 4 and 5). Reduction of Benzo[h]quinoline **1f** required 84 h to reach an average yield of 51% (Table 2, entry 6). Hydrogenation of 2-methyl-indole **1g** required 61 h and the use of a stoichiometric amount of (*R*)-(-)- Camphor-10-sulfonic acid [56,57] allowed to reach a 65% yield (Table 2, entry 7). The hydrogenation of 2-chloro-quinoline **1h** led exclusively to the dechlorinated product **2h**, suggesting the catalyst may be used for removal of chloride substituents from aromatic and aliphatic organic contaminants (Table 2, entry 8). Finally, 8-hydroxyquinoline **1i** and benzo[f]quinoline **1j** were less reactive to hydrogenation with only 24% and 11% yields obtained respectively after an extended time of 61 h (Table 2, entries 9-10).

Overall, considering previous studies applying copper/Al_2O_3 heterogeneous catalysts to the hydrogenation of N-heterocycles [58,59], the present catalyst operates at a rather high

copper loading (9.2 mol%) then previously reported (2.5 mol%). The reactions require higher hydrogen pressures and longer reaction times to be effective (50 bar H_2 and 13-84 h versus 40 bar H_2 and 24 h), leading to lower turnover frequencies (TOF between 0.02-0.83 h^{-1} versus 1.50-1.70 h^{-1}). Moreover, commercially available Pd/C was previously found active to catalyze the hydrogenation of quinolines but could not be recycled effectively (60°C, 20 bar H_2, water, 1 h, 78% yield, TOF 130.0 h^{-1}) [60]. Pt/C followed the same trend but better catalysts were developed working on two strategies: the size effect and electronic metal-support interaction (EMSI). The use of single-atom site (SA) copper catalysts on N-doped carbon materials has also been reported [61]. SA Cu/N-doped carbon supported on TiO_2 host (Cu_1/CN/TiO_2) could afford a high catalytic performance (a 94% yield of target product) under more mild reaction conditions (60 °C, 2 h, H_3N-BH_3 as hydrogen donor), but the high activity relied on using TiO_2 as a host to benefit the formation of doped pyrrolic-N, which increased the complexity of the catalyst system [62].

Afterwards, **CuNC-1-700** catalyst was successfully applied to catalyse the selective hydrogenation of compounds containing various C=C and C≡C bonds (Tables 3 and 4). The performed hydrogenation reactions were completely selective without any semihydrogenation or condensation by-products. Under a hydrogen gas pressure of 10 bar at 80 °C, alkenes **3a-d** bearing aromatic and/or aliphatic substituents were all hydrogenated quantitatively to the corresponding alkanes within 13 h (Table 3, entries 1-4). Cyclohexene **3e** was also quantitatively hydrogenated to cyclohexane (Table 3, entry 5) but phenylcyclohexene **3f**, a tri-substituted alkene, was found less reactive, because of its steric hindrance [63], hydrogenated product **4f** being obtained in a 46% yield after a longer reaction time of 64 h (Table 3, entry 6).

Finally, hydrogenation of alkynes **5a-d** to the corresponding alkanes **4a,c,d,g** was also achieved in quantitative yields within 13 h (Table 4, entries 1-4). The selective formation of alkane derivatives **4a,c,d,g** was observed without the presence of any unsaturated intermediates even in the case of bulky diphenyl acetylene.

In order to better understand the long-term stability of these copper supported catalysts, we have also investigated the possible recycling of **CuNC-1-700** catalyst. The solid catalyst was recovered and reused up to three cycles for the hydrogenation of trans-stilbene **3d** (Scheme 2). The yield decreases gradually from 99% in the first run to 42% in the third cycle, indicating a significant loss of its catalytic activity. The hot filtration experiment was performed to evaluate the heterogeneity and catalyst stability. As shown in Fig. S10, the conversion of quinoline remained constant after the removal of the catalyst, indicating that the reaction stopped without the presence of the active phase. ICP-AES analysis of the reaction solution after test demonstrated an absence of solubilized copper, confirming no leaching of copper species was occurring or to a level below the detection limit of the ICP-AES. TEM images (Fig. S11) of the three-time used **CuNC-1-700** catalyst show a significant increase in the size of copper nanoparticles from 29 nm to more than 100 nm, with the disappearance of small copper nanoparticles (less than 2 nm), indicating the sintering of copper nanoparticles during the reaction, which is probably the main reason for the catalyst deactivation.

Table 2. Catalytic performance of the **CuNC-1-700** for the hydrogenation of N-heterocycles

Entry	Substrate	Product	t (h)	Yield (%)[a],[b]	TOF (h^{-1})[c]
1	 1a	 2a	61	82	0.15
2	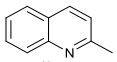 1b	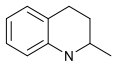 2b	61	77	0.14
3	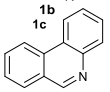 1c	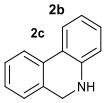 2c	61	75	0.18
4	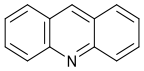 1d	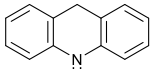 2d	13	99	0.83
5	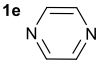 1e	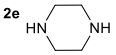 2e	13	81	0.68
6	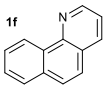 1f	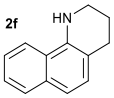 2f	84	51	0.11
7	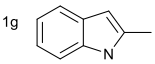 1g	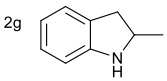 2g	61	65[d]	0.12
8	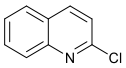 1h	 2a	13	77	0.64
9	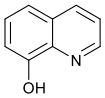 1i	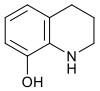 2i	61	24	0.04
10	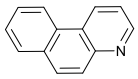 1j	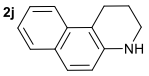 2j	61	11	0.02

[a] Reaction conditions: substrate (0.7 mmol), catalyst (0.010 g, 0.065 mmol Cu, 9.2 mol% Cu), iPrOH (4.0 mL), H_2 (50 bar), T (80 °C).

[b] Determined by GC and GC-MS.

[c] Turnover frequency = mol of product/mol of catalyst/hour.

[d] Reaction performed in the presence of 1 equivalent of (R)-(-)-Camphor-10-sulfonic acid. No reaction without.

Table 3. Catalytic performance of the **CuNC-1-700** for the hydrogenation of alkenes.

Entry	Substrate	Product	t (h)	Yield(%) [a][b]
1	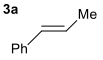		13	>99
2			13	>99
3			13	>99
4			13	>99
5			16	>99
6			64	46

[a] Reaction conditions: substrate (0.7 mmol), catalyst (0.005 g, 0.032 mmol Cu, 4.6 mol% Cu), iPrOH (4.0 mL), H_2 (10 bar), T (80 °C). [b] Determined by GC and GC-MS.

Table 4. Catalytic performance of the **CuNC-1-700** for the hydrogenation of alkynes.

Entry	Substrate	Product	Yield (%) [a][b]
1	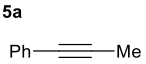	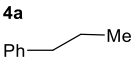	>99
2	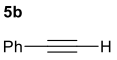	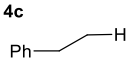	>99
3	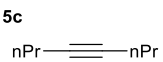	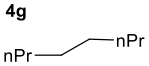	>99
4	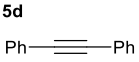	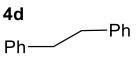	>99

[a] Reaction conditions: substrate (0.7 mmol), catalyst (0.005 g, 0.032 mmol Cu, 4.6 mol% Cu), iPrOH (4.0 mL), H_2 (10 bar), T (80 °C), t (13 h). [b] Determined by GC and GC-MS.

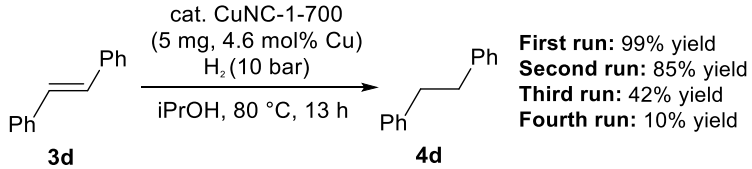

Scheme 2. Hydrogenation of trans-stilbene **3d** with recycling of **CuNC-1-700** catalyst. Copper content before three cycles: 41 wt.%; copper content after three cycles: 41wt.%.

Very few studies have been reported on the mechanism of the hydrogenation of quinoline to date. The reaction mechanism may be associated with the nature of the active metals, the support properties and the polarity of the reaction solvent, etc.[64,65]. The dissociation of hydrogen over the solid Cu surface involves H-H splitting through homolytic pathway, generating two hydrogen atoms adsorbed on copper surface sites [66]. The adsorption of quinoline on the catalyst surface is supposed to proceed through π-π stacking, considering that the NC support contains many organic groups and the aromatic structure in backbone which facilitate the affinity for quinoline [67]. However, because the quinoline hydrogenation was performed in the polar protic iPrOH, the π-π stacking interactions between the aromatic structure of the NC support and the aromatic ring of quinoline are weaker than the hydrogen bondings between the aromatic ring and iPrOH. Besides, the adsorption of quinoline on the surface of the catalyst is generally achieved by the coordination between the nitrogen atom of quinoline and the active metal, which facilitates the formation of the product **2a**. The high selectivity we observed is thus related to the use of protic iPrOH, a further hydrogenation being inhibited by the interactions of the π electrons of **2a** aromatic ring with the protons of the solvent [68]. In addition, the study on the effect of hydrogen pressure on quinoline hydrogenation, as presented in Table S4, showed a strong dependence of the reaction rate on the hydrogen pressure, which indicates that the hydrogen dissociation acts as the rate-limiting step with the **CuNC-1-700** catalyst. Based on these facts, a plausible reaction mechanism for quinoline hydrogenation over **CuNC-1-700** was thus proposed and presented in Scheme 3.

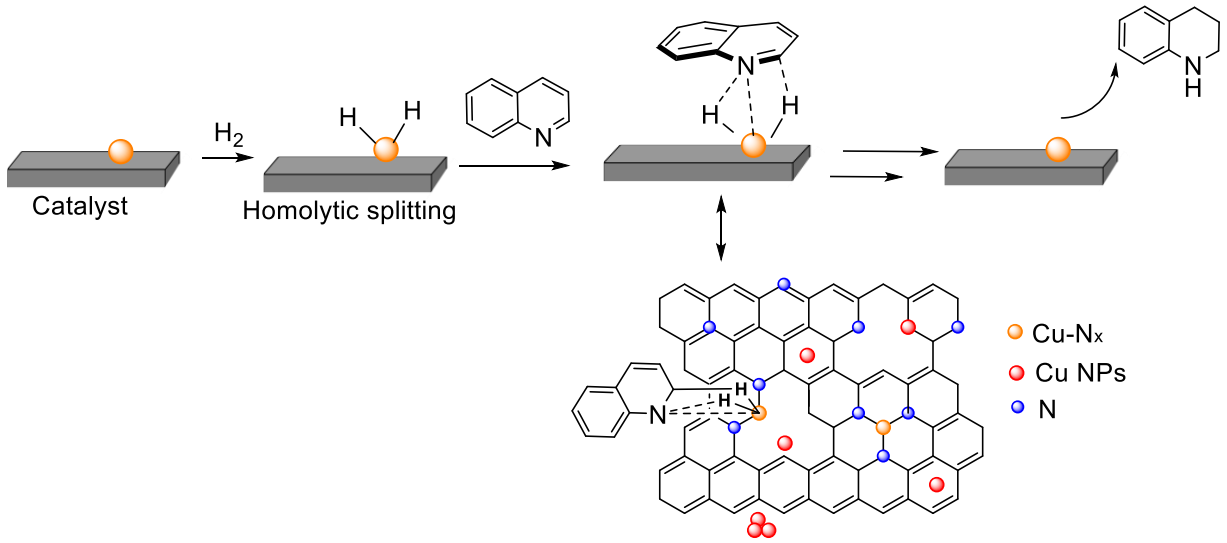

Scheme 3. Plausible reaction mechanism for quinoline hydrogenation.

3. CONCLUSIONS

Herein, we developed an original approach based on reticular chemistry of chitosan, melamine and ethylene diamine tetraacetic acids followed by carbonization to entrap copper bursts inside hierarchical porous carbon framework. The efficiency of this approach lies in the possibility to prepare dispersed metals with up to 52 wt% loading in the case of copper. The presence of nitrogen as metal stabilizer and the cross-linking were pivotal to access copper supported on hierarchically-porous network. Interesting hydrogenation activities were observed for unsaturated double and triple carbon-carbon bonds and even for challenging N-heterocycles with quantitative to average yields. Comparatively, the catalyst prepared using alginate displays poor catalytic activity, owing to the lack of ligand-stabilization around copper nanoparticles, thereby highlighting the importance of incorporating nitrogen in the framework of carbon support. The copper catalysts are demonstrating limited stability in reaction, with a decrease of the activity by ~60% after 3

reaction cycles, a deactivation associated to the copper nanoparticles aggregation and growth. Despite the lack in stability associated to the presence of copper, this reticular chemistry approach can be expanded to encapsulate a large panel of affordable metals on heterogeneous carbon-based catalysts.

Acknowledgments

The Chevreul Institute is thanked for its help in the development of this work through the ARCHI-CM project supported by the "Ministère de l'Enseignement Supérieur de la Recherche et de l'Innovation", the region "Hauts-de-France", the ERDF program of the European Union and the "Métropole Européenne de Lille. The authors would like to thank Martine Trentesaux and Pardis Simon for their help in carrying out the work on the Surface Analysis facility, Laurence Burylo from the X Ray diffraction and diffusion facility of the Advanced Characterization Platform of the Chevreul Institute. We also thank Olivier Gardoll (UCCS) for physical characterization support and Céline Delabre (UCCS) for GC and GC-MS analyses. We thank Hervé Vezin (LASIR) for the CW EPR analysis and data processing. NH thanks UEMF for scholarship. SR, AEK and NH acknowledge Programme Hubert Curien – Toubkal (project No.18/40) for supporting and funding partially this work.

References

[1] A. J. Marchi, J. L. G. Fierro, J. Santamaría, A. Monzón, Dehydrogenation of isopropylic alcohol on a Cu/SiO_2 catalyst: a study of the activity evolution and reactivation of the catalyst, Appl. Catal. A 142 (1996) 375–386.

[2] P. Mäki-Avela, J. Hájek, T. Salmi, D. Yu Murzin, Chemoselective hydrogenation of carbonyl compounds over heterogeneous catalysts, Appl. Catal. A 292 (2005) 1–49.

[3] M. J. Suh, S. K. Ihm, Preparation of Copper Oxide with High Surface Area Associated with Mesoporous Silica,Top. Catal. 53 (2010) 447–454.

[4] X. M. Liu, G. Q. Lu, Z. F. Yan, J. Beltramini, Recent Advances in Catalysts for Methanol Synthesis via Hydrogenation of CO and CO_2, Ind. Eng. Chem. Res. 42 (2003) 6518–6530.

[5] J. Gong, H. Yue, Y. Zhao, S. Zhao, L. Zhao, J. Lv, S. Wang, X. Ma, Synthesis of ethanol via syngas on Cu/SiO_2 catalysts with balanced Cu^0-Cu^+ sites, J. Am. Chem. Soc. 134 (2012) 13922-13925.

[6] Q. Q. Zhang, J. Dong, Y. M. Liu, Y. Cao, H. Y. He, Y. D. Wang, An efficient noble-metal-free supported copper catalyst for selective nitrocyclohexane hydrogenation to cyclohexanone oxime, Chem Commun. 53 (2017) 2930-2933.

[7] D. Y. Osadchii, A. I. Olivos-Suarez, A. V. Bavykina, J. Gascon, Revisiting Nitrogen Species in Covalent Triazine Frameworks, Langmuir 33 (2017) 14278-14285.

[8] J. Feng, G. Chuanbo, Y. Yadong, Stabilization of noble metal nanostructures for catalysis and sensing, Nanoscale 10 (2018) 20492- 20504.

[9] R. M. Bullock, Abundant Metals Give Precious Hydrogenation Performance, Science 342 (2013) 1054–1055.

[10] R.H. Morris, Iron Group Hydrides in Noyori Bifunctional Catalysis, Chem. Record, 16 (2016) 2640–2654.

[11] J. R. Ludwig, C. S. Schindler, Catalyst: Sustainable Catalysis, Chem 2 (2017) 313–316.

[12] F. Kallmeier, R. Kempe, Manganese Complexes for (De)Hydrogenation Catalysis: A Comparison to Cobalt and Iron Catalysts, Angew. Chem. Int. Ed. 57 (2018) 46–60.

[13] F. Agbossou-Niedercorn, C. Michon, Bifunctional homogeneous catalysts based on first row transition metals in asymmetric hydrogenation, Coord. Chem. Rev. 425 (2020) 213523.

[14] F. Chen, B. Sahoo, C. Kreyenschulte, H. Lund, M. Zeng, L. He, K. Junge, M. Beller, Selective cobalt nanoparticles for catalytic transfer hydrogenation of N-heteroarenes, Chem. Sci. 8 (2017) 6239-6246.

[15] S. Frindy, A. El Kadib, M. Lahcini, A. Primo, H. García, Copper Nanoparticles Stabilized in a Porous Chitosan Aerogel as a Heterogeneous Catalyst for C−S Cross-coupling, ChemCatChem 7 (2015) 3307-3315.

[16] K. Yoshida, C. Gonzalez-Arellano, R. Luque, P. L. Gai, Efficient hydrogenation of carbonyl compounds using low-loaded supported copper nanoparticles under microwave irradiation, Appl. Catal. A 379 (2010) 8-44.

[17] L. Chen, H. Wang, C. Liu, X. Liu, S. Xing, One-pot achieving well-dispersed copper nanoparticles on N-doped carbon films, J. Alloys Compd. 656 (2016) 622-627.

[18] A. Dhakshinamoorthy, S. Navalon, D. Sempere, M. Alvaro, H. Garcia, Aerobic Oxidation of Thiols Catalyzed by Copper Nanoparticles Supported on Diamond Nanoparticles, ChemCatChem, 5 (2013) 241-246.

[19] A. Dhakshinamoorthy, A. M. Asiri, H. Garcia, Formation of C−C and C−Heteroatom Bonds by C−H Activation by Metal Organic Frameworks as Catalysts or Supports, ACS Catalysis 9 (2019) 1081-1102.

[20] S. R. Chaurasia, B.M. Bhanage, One-pot synthesis of symmetrical and asymmetrical diphenylamines from guanidines with aryl iodide using Cu/Cu_2O nanocatalyst, Molecular Catalysis 492 (2020) 110992-111004.

[21] S. Chen, R. Wojcieszk, F. Dumeignil, E. Marceau, S. Royer, How Catalysts and Experimental Conditions Determine the Selective Hydroconversion of Furfural and 5-Hydroxymethylfurfural, Chem. Rev. 118 (2018) 11023-11117.

[22] A. Dhakshinamoorthy, S. Navalon, D. Sempere, M. Alvaro, H. Garcia, Reduction of alkenes catalyzed by copper nanoparticles supported on diamond nanoparticles, Chem. Commun. 49 (2013), 2359-2361.

[23] N. Nagarjun, K. Arthy, A. Dhakshinamoorthy, Copper(II)-Doped ZIF-8 as a Reusable and Size Selective Heterogeneous Catalyst for the Hydrogenation of Alkenes using Hydrazine Hydrate, Eur. J. Inorg. Chem. 2021 (2021) 2108–2119.

[24] V. G. Ramu, A. Bordoloi, T. C. Nagaiah, W. Schuhmann, M. Muhler, C. Cabrele, Copper nanoparticles stabilized on nitrogen-doped carbon nanotubes as efficient and recyclable catalysts for alkyne/aldehyde/cyclic amine A(3)-type coupling reactions, Appl. Catal. A 431 (2012) 88-94.

[25] R. V. Siva Prasanna Sanka, Y. Leterrier, S. Pandey, M. Srivastava, A. Srivastava, W. H. Binder, S. Rana, V. Michaud, Nitrogen-doped graphene stabilized copper nanoparticles for Huisgen [3+2] cycloaddition “click” chemistry, Chem. Commun. 55 (2019) 6249-6252.

[26] N. Renfeng, M. Meng, D. Weichen, S. Juanjuan, L. Yingchun, H. Zhaoyin, Selective hydrogenation of Cdouble bondC bond over N-doped reduced graphene oxides supported Pd catalyst, Appl. Catal. B 180 (2016) 607-613.

[27] N. Hammi, S. Chen, F. Dumeignil, S. Royer, A. El Kadib, Chitosan as a sustainable precursor for nitrogen-containing carbon nanomaterials: synthesis and uses, Materials Today Sustainability 10 (2020) 100053.

[28] L. Liu, A. Corma, Metal Catalysts for Heterogeneous Catalysis: From Single Atoms to Nanoclusters and Nanoparticles, Chem. Rev. 118 (2018) 4981-5079.

[29] J. Zhang, C. Zheng, M. Zhang, Y. Qiu, Q. Xu, W-C. Cheong, W. Chen, L. Zheng, L. Gu, Z. Hu, D. Wang, Y. Lie, Controlling N-doping type in carbon to boost single-atom site Cu catalyzed transfer hydrogenation of quinoline, Nano Res. 13 (2020) 3082–3087.

[30] F. Hao, J. Zheng, S. He, H. Zhang, P. Liu, H. Luo, W. Xiong, One-step complexed preparation of nitrogen and Cu co-doped oxidative active carbon catalysts Cu-N/OAC for furfural selective hydrogenation with high yield, Catal. Commun. 151 (2021) 106266.

[31] F. Chen, B. Sahoo, C. Kreyenschulte, H. Lund, M. Zeng, L. He, K. Junge, M. Beller, Selective cobalt nanoparticles for catalytic transfer hydrogenation of N-heteroarenes, Chem. Sci. 8 (2017) 6239-6246;

[32] F. Chen, A-E. Surkus, L. He, M-M. Pohl, J. Radnik, C. Topf, K. Junge, M. Beller, Selective Catalytic Hydrogenation of Heteroarenes with N-Graphene-Modified Cobalt Nanoparticles (Co_3O_4–Co/NGr@α-Al_2O_3), J. Am. Chem. Soc. 137 2015 11718–11724;

[33] K. Murugesan, T. Senthamarai, A. S. Alshammari, R. M. Altamimi, C. Kreyenschulte, M-M. Pohl, H. Lund, R.V. Jagadeesh, M. Beller, Cobalt-Nanoparticles Catalyzed Efficient and Selective Hydrogenation of Aromatic Hydrocarbons, ACS Catal. 9 (2019) 8581–8591.

[34] S. Deguchi, K. Tsujii, K. Horikoshi, In situ microscopic observation of chitin and fungal cells with chitinous cell walls in hydrothermal conditions, Sci. Rep. 5 (2015) 11907.

[35] S.A. Nicolae, H. Au, P. Modugno, H. Luo, A. E. Szego, M. Qiao, L. Li, W. Yin, H. J. Heeres, N. Berged, M.-M. Titirici, Recent advances in hydrothermal carbonisation: from tailored carbon materials and biochemicals to applications and bioenergy, Green. Chem. 22 (2020) 4747-4800.

[36] N. Hammi, N. Marcotte, M. Marinovae, K. Draoui, S. Royer, A. El Kadib, Nanostructured metal oxide@carbon dots through sequential chitosan templating and carbonisation route, ACS Appl. Bio Mater. 2 (2019) 61-69.

[37] S. Moosvi, K. Majid, T. Ara, Studying the electrical, thermal, and photocatalytic activity of nanocomposite of polypyrrole with the photoadduct of K3[Fe(CN)6] and diethylenetriamine, Mat. Res. 19 (2016) 983-990.

[38] J. F. Zhang, R. Zhong, Q. Zhou, X. Hong, S. Huang, H. Z. Cui, X. F. Hou, Recyclable Silica-Supported Iridium Catalysts for Selective Reductive Transformation of Quinolines with Formic Acid in Water, ChemCatChem 9 (2017) 2496-2505.

[39] Y. Yi, Y. Zhang, Y. Wang, L. Shen, M. Jia, Y. Huang, Z. Hou, G. Zhuang, Ethylenediaminetetraacetic acid as capping ligands for highly water-dispersible iron oxide particles, Nanoscale. Res. Lett 9 (2014) 27.

[40] J. Zhang, X. Liu, W. Chen, H. Fang, Y. Zheng, Y. Yuan, N configuration control of N-doped carbon for stabilizing Cu nanoparticles: The synergistic effects on oxy-carbonylation of methanol, Carbon 158 (2020) 836-845.

[41] O. Jennah, R. Beniazza, C. Duboc, T. Buffeteau, A. El Kadib, D. Lastécouères, M. Lahcini, J. M. Vincent, Photoredox Catalysis at Copper(II) on Chitosan: Application to Photolatent CuAAC, Adv. Synth. Catal. 360 (2018) 4615-4624.

[42] L. Roldán, L. Truong-Phuoc, A. Ansón-Casaos, C. Pham-Huu, E. García-Bordejé, Mesoporous carbon doped with N,S heteroatoms prepared by one-pot auto-assembly of molecular precursor for electrocatalytic hydrogen peroxide synthesis, Catal. Today. 301 (2018) 2-10.

[43] D. A. Bulushev, A. L.Chuvilin, V. I. Sobolev, S. G. Stolyarova, Y. V. Shubin, I. P. Asanov, A.V. Ishchenko, G. Magnani, M. Riccò, A.V. Okotrub, L. G.Bulusheva, Copper on carbon materials: stabilization by nitrogen doping, J. Mater. Chem. A 5 (2017) 10574-10583.

[44] H.Tian, C. Zhangn, P. Su, Metal-organic-framework-derived formation of Co–N-doped carbon materials for efficient oxygen reduction reaction, J. Energy Chem. 40 (2020) 137-143.

[45] R. Liu, D. Wu, X. Feng, K. Müllen, Nitrogen-Doped Ordered Mesoporous Graphitic Arrays with High Electrocatalytic Activity for Oxygen Reduction, Angew. Chem. Int. Ed. 49 (2010) 2565-2569.

[46] X. Zhao, H. Yang, P. Jing, W. Shi, G. Yang, P. Cheng, A Metal-Organic Framework Approach toward Highly Nitrogen-Doped Graphitic Carbon as a Metal-Free Photocatalyst for Hydrogen Evolution, Small 13 (2017) 1603279−1603284.

[47] K. Sun, S. Sun, C. Zhu, H. Tian, H. Yang, J. Li, Hidden CDW states and insulator-to-metal transition after a pulsed femtosecond laser excitation in layered chalcogenide 1T-$TaS_{2-x}Se_x$, Sci. Adv. 4 (2018) 9660−9666.

[48] A. Ganguly, S. Sharma, P. Papakonstantinou, J. Hamilton, Probing the Thermal Deoxygenation of Graphene Oxide Using High-Resolution In Situ X-ray-Based Spectroscopies, J. Phys. Chem. C 115 (2011) 17009-17019.

[49] Y. Li, X. Cai, S. Chen, H. Zhang, K. H L Zhang, J. Hong, B. Chen, D. H. Kuo, W. Wang, Highly Dispersed Metal Carbide on ZIF-Derived Pyridinic-N-Doped Carbon for CO_2 Enrichment and Selective Hydrogenation, ChemSusChem 11 (2018) 1040-1047.

[50] A. Aijaz, N. Fujiwara, Q. Xu, From Metal–Organic Framework to Nitrogen-Decorated Nanoporous Carbons: High CO2 Uptake and Efficient Catalytic Oxygen Reduction, J. Am. Chem. Soc. 136 (2014) 6790 – 6793.

[51] G. Águila, F. Gracia and P. Araya, CuO and CeO 2 catalysts supported on Al 2O 3, ZrO 2, and SiO 2 in the oxidation of CO at low temperature, Appl. Catal. A: Gen. 343 (2008) 16–24.

[52] C. Li, J. Xie, J. Zhang, B. Dai, Nitrogen-Modified Activated Carbon Supported Cu(II)Cu(I)/NAC Catalysts for Gas–Solid Acetylene Dimerization,Catal. Lett. 151 (2021) 2990–2995.

[53] B. Wang, V. Likodimos, A. J. Fielding, R. A. W. Dryfe, In situ Electron paramagnetic resonance spectroelectrochemical study of graphene-based supercapacitors: Comparison between chemically reduced graphene oxide and nitrogen-doped reduced graphene oxide, Carbon 160 (2020) 236-246.

[54] Y. Yang, L. Jia, B. Hou, D. Li, J. Wang, Y. Sun, The Correlation of Interfacial Interaction and Catalytic Performance of N-Doped Mesoporous Carbon Supported Cobalt Nanoparticles for Fischer−Tropsch Synthesis, J. Phys. Chem. C 118 (2014) 268–277.

[55] A. N. Kim, B. M. Stoltz, Recent Advances in Homogeneous Catalysts for the Asymmetric Hydrogenation of Heteroarenes, ACS Catal. 10 (2020) 13834−13851.

[56] D. S. Wang, J. Tang, Y. G. Zhou, M. W. Chen, C. B. Yu, Y. Duana, G. F. Jiang, Dehydration triggered asymmetric hydrogenation of 3-(α-hydroxyalkyl)indoles, Chem. Sci. 2 (2011) 803–806.

[57] Y. Duan, L. Li, M. W. Chen, C. B. Yu, H. J. Fan, Y. G. Zhou, Homogenous Pd-catalyzed asymmetric hydrogenation of unprotected indoles: scope and mechanistic studies, J. Am. Chem. Soc. 136 (2014) 7688–7700.

[58] W. Li, X. Cui, K. Junge, A.-E. Surkus, C. Kreyenschulte, S. Bartling, M. Beller, General and Chemoselective Copper Oxide Catalysts for Hydrogenation Reactions, ACS Catal. 9 (2019) 4302−4307.

[59] P. Ryabchuk, M. Anwar, S. Dastgir, K. Junge, M. Beller, From Mobile Phones to Catalysts: E-Waste-Derived Heterogeneous Copper Catalysts for Hydrogenation Reactions, ACS Sustainable Chem. Eng. 9 (2021) 10062−10072.

[60] H. Mao, C. Chen, X. Liao, B. Shi, Catalytic hydrogenation of quinoline over recyclable palladium nanoparticles supported on tannin grafted collagen fibers, J. Mol. Cat. A: Chem. 341 (2011) 51-56.

[61] Z. Wei, F. Shao, J. Wang, Recent advances in heterogeneous catalytic hydrogenation and dehydrogenation of N-heterocycles, Chinese Journal of Catalysis 40 (2019) 980-1002.

[62] J. Zhang, C. Zheng, M. Zhang, Y. Qiu, Q. Xu, W.C. Cheong, W. Chen, L. Zheng, L. Gu, Z. Hu, D. Wang, Y. Li, Controlling N-doping type in carbon to boost single-atom site Cu catalyzed transfer hydrogenation of quinoline, Nano Res. 13 (2020) 3082-3087.

[63] P. Viereck, S. Krautwald, T. P. Pabst, P. J. Chirik, A Boron Activating Effect Enables Cobalt-Catalyzed Asymmetric Hydrogenation of Sterically Hindered Alkenes, J. Am. Chem. Soc. 142 (2020) 3923-3930.

[64] M. M. Dell'Annaa, V. F. Capodiferro, M. Mali, D. Manno, P. Cotugno, A. Monopoli, P. Mastrorilli, Highly selective hydrogenation of quinolines promoted by recyclable polymer supported palladium nanoparticles under mild conditions in aqueous medium, Appl. Catal. A: Gen. 481 (2014) 89-95.

[65] M. Fang, N. Machalaba, R. A. Sánchez-Delgado, Hydrogenation of arenes and N-heteroaromatic compounds over ruthenium nanoparticles on poly(4-vinylpyridine): a versatile catalyst operating by a substrate-dependent dual site mechanism, Dalton Trans. 40 (2011) 10621-10632.

[66] C. Xu, G. Chen, Y. Zhao, P. Liu, X. Duan, L. Gu, G. Fu, Y. Yuan, N. Zheng, Interfacing with silica boosts the catalysis of copper. Nat. Commun. 9 (2018) 3367.

[67] D. Zhu, H. Jiang, L. Zhang, X. Zheng, H. Fu, M. Yuan, H. Chen, R. Li, Aqueous Phase Hydrogenation of Quinoline to Decahydroquinoline Catalyzed by Ruthenium Nanoparticles Supported on Glucose-Derived Carbon Spheres, ChemCatChem 6 (2014) 2954-2960.

[68] B. Sun, F. A. Khan, A. Vallat, G. Süss-Fink, NanoRu@hectorite: A heterogeneous catalyst with switchable selectivity for the hydrogenation of quinoline, Appl. Catal. A: Gen. 467 (2013) 310-314.